Fuel Cycle Research and Development
Document Cover Sheet

Name/Title of Deliverable/Milestone	M3503040403 / Complete joint summary report for FY10 activities
Work Package Title and Number	SR1015030404 Alternative Waste Forms for Fission Products
Work Package WBS Number	1.5.03.04
Responsible Work Package Manager	Paul Filpus-Luyckx *(signature)*
	(Name/Signature)

Date Submitted 9/24/10

Quality Rigor Level for
Deliverable/Milestone
⊠ Rigor Level 3 ☐ Rigor Level 2 ☐ Nuclear Data

This deliverable was prepared in accordance with   SRNL
_____
(Participant's (National Laboratory or Subcontractor) Name)
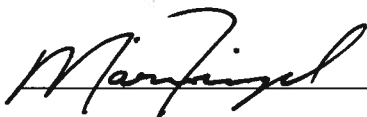
QA program which meets the requirements of

⊠ DOE Order 414.1 ☐ Nuclear Data Requirements

This Deliverable was subjected to:

⊠ Independent Technical Review   ☐ Peer Review

Independent Technical Review (ITR)	Peer Review (PR)	Nuclear Data Validation (NDV)
Review Documentation Provided	**Review Documentation Provided**	**Review Documentation Provided**
☐ Signed ITR Report or,	☐ Signed PR Report or,	☐ Signed Validation Documentation or,
☐ Signed ITR Concurrence Sheet or,	☐ Signed PR Concurrence Sheet or,	☐ Signed Validation Concurrence or,
⊠ Signature of ITR Reviewer(s) below	☐ Signature of PR Reviewer(s) below	☐ Signature of Validation Reviewer(s) below,

Name and Signature of Peer Reviewers(s)/Independent Technical Reviewer(s) (NOTE: Electronic signatures or other proof of approval (e-mails, other electronic verification) may be provided in lieu of signatures on this form)

(signature)
_____   _____

Preliminary Study of Ceramics for Immobilization of Advanced Fuel Cycle Reprocessing Wastes

Fuel Cycle Research & Development

A.L. Billings, K.S. Brinkman, K.M. Fox,
and J.C. Marra
Savannah River National Laboratory
M. Tang and K.E. Sickafus
Los Alamos National Laboratory

SUMMARY

The Savannah River National Laboratory (SRNL) developed a series of ceramic waste forms for the immobilization of Cesium/Lanthanide (CS/LN) and Cesium/Lanthanide/Transition Metal (CS/LN/TM) waste streams anticipated to result from nuclear fuel reprocessing. Simple raw materials, including Al_2O_3, CaO, and TiO_2 were combined with simulated waste components to produce multiphase ceramics containing hollandite-type phases, perovskites (particularly $BaTiO_3$), pyrochlores, zirconolite, and other minor metal titanate phases. Identification of excess Al_2O_3 via X-ray Diffraction (XRD) and Scanning Electron Microscopy with Energy Dispersive Spectroscopy (SEM/EDS) in the first series of compositions led to a Phase II study, with significantly reduced Al_2O_3 concentrations and increased waste loadings.

Three fabrication methodologies were used, including melting and crystallizing, pressing and sintering, and Spark Plasma Sintering (SPS), with the intent of studying phase evolution under various sintering conditions. XRD and SEM/EDS results showed that the partitioning of the waste elements in the sintered materials was very similar, despite varying stoichiometry of the phases formed. The Phase II compositions generally contained a reduced amount of unreacted Al_2O_3 as identified by XRD, and had phase assemblages that were closer to the initial targets. Chemical composition measurements showed no significant issues with meeting the target compositions. However, volatilization of Cs and Mo was identified, particularly during melting, since sintering of the pressed pellets and SPS were performed at lower temperatures. Partitioning of some of the waste components was difficult to determine via XRD. SEM/EDS mapping showed that those elements, which were generally present in small concentrations, were well distributed throughout the waste forms.

Initial studies of radiation damage tolerance using ion beam irradiation at Los Alamos National Laboratory (LANL) showed little if any modification of the material after irradiation. Additional study in this area is needed. Chemical durability was briefly studied using the Product Consistency Test (PCT). Most of the elements measured were retained by the ceramic waste forms, indicating good chemical durability. Cs, Mo, and Rb were released at somewhat higher rates as compared to the matrix components, although benchmark compositions and additional characterization are needed in order to qualify the PCT results.

CONTENTS

FIGURES

TABLES

ABBREVIATIONS

AD	Analytical Development
AFCI	Advanced Fuel Cycle Initiative
ARM	Approved Reference Material
CCIM	Cold Crucible Induction Melter
CS	Cesium/Strontium waste stream
DOE	Department of Energy
EA	Environmental Assessment
EDS	Energy Dispersive Spectroscopy
FCR&D	Fuel Cycle Research and Development
HLW	High Level Waste
ICP-AES	Inductively Coupled Plasma – Atomic Emission Spectroscopy
ICP-MS	Inductively Coupled Plasma – Mass Spectroscopy
LANL	Los Alamos National Laboratory
LN	Lanthanide waste stream
NM	Noble Metals
PCT	Product Consistency Test
PNNL	Pacific Northwest National Laboratory
SEM	Scanning Electron Microscopy
SPS	Spark Plasma Sintering
SRNL	Savannah River National Laboratory
TALSPEAK	Trivalent Actinide - Lanthanide Separation by Phosphorous reagent Extraction from Aqueous Komplexes
TM	Transition Metal fission product waste stream
TRUEX	TRansUranic EXtraction
XRD	X-ray Diffraction

ACKNOWLEDGEMENTS

1. INTRODUCTION

Efforts being conducted by the United States Department of Energy (DOE) under the Fuel Cycle Research and Development (FCR&D) program are aimed at demonstrating a proliferation-resistant, integrated nuclear fuel cycle. The envisioned fuel reprocessing technology would separate the fuel into several fractions, thus partitioning the waste into groups with common chemistry. With these partitioned waste streams, it is possible to treat waste streams separately or combine waste streams for treatment when it is deemed appropriate. A trade study conducted in 2008 concluded that it was beneficial from a cost perspective to combine waste streams and treat them using existing waste form technologies.[1] A borosilicate glass was identified as the preferred waste form for the Cs/Sr (CS), lanthanide (LN) and transition metal fission product (TM) combined waste stream. Unfortunately, several fission products (e.g. noble metals and molybdenum) have limited solubility in borosilicate glasses. Therefore, the use of borosilicate glass may simplify waste form processing but result in significant increases in waste form volumes. This would defeat a major advanced fuel cycle reprocessing objective of minimizing high level waste form volumes.

A joint fiscal year 2009 study by the Pacific Northwest National Laboratory (PNNL) and the Savannah River National Laboratory (SRNL) developed baseline borosilicate glass waste forms for three projected waste streams resulting from the Advanced Fuel Cycle Initiative (AFCI) aqueous separations process.[2] While the study identified acceptable glass compositions for a CS/LN/TM with high MoO_3 waste composition and a CS/LN/TM with high noble metals (NM) waste composition, the waste loading was found to be limited by both Mo and NM concentrations. Additionally, several of the glasses fabricated for the CS/LN-only waste composition underwent massive crystallization upon slow cooling. Chemical durability testing indicated the excellent leaching resistance of these crystalline materials, with many of the crystallized glasses having better leaching resistance than the amorphous glass compositions developed for the other waste streams. A recently completed Laboratory Directed Research and Development project at PNNL also showed promising results in the development of glass-ceramic waste forms for these waste types.

Based on these observations, the team developed a renewed interest in exploring crystalline-type waste forms either in a completely crystalline phase assemblage or as crystalline phases within a glassy matrix, which became the focus for fiscal year 2010 studies. This report documents studies completed at SRNL on ceramic (i.e., fully crystallized) waste forms, with characterization completed in collaboration with Los Alamos National Laboratory (LANL). The work at PNNL focused on glass-ceramic systems, which will be documented separately.

Titanate ceramics have been thoroughly studied for use in immobilizing nuclear wastes (e.g., the SYNROC family) due to their natural resistance to leaching in water.[3, 4] Assemblages of several titanate phases have been successfully demonstrated to incorporate radioactive waste elements, and the multiphase nature of these materials allows them to accommodate variation in the waste composition.[5] While these materials are typically densified via hot isostatic pressing, recent work has shown that they can also be produced from a melt. For example, demonstrations have been completed using the Cold Crucible Induction Melter (CCIM) technology to produce several crystalline ceramic waste forms, including murataite-rich ceramics,[6] zirconolite/pyrochlore ceramics,[7] Synroc-C (zirconolite, hollandite, perovskite),[8] aluminotitanate ceramics, and zirconia.[9] This production route is advantageous since melters are already in use for defense high level waste (HLW) vitrification in several countries, and melter technology greatly reduces the potential for airborne contamination as compared to powder handling operations.

The primary goal of the fiscal year 2010 studies at SRNL was to identify ceramic compositions that effectively accommodate characteristic wastes generated from nominal advanced fuel cycle reprocessing

scenarios. A second objective was to provide preliminary characterization and performance data on specific properties of interest for these waste forms. Ceramic waste forms incorporate the radionuclides in the waste as part of their crystalline structure. As such, ceramic forms are tailored to create certain minerals (i.e. unique crystalline structures) that will host the radionuclides by binding them at specific sites within their crystalline structure. These synthetic minerals are made to reflect natural minerals that host natural radioactive species such as uranium, nonradioactive isotopes of the fission products, or both. Tailoring of a ceramic waste form is based on the knowledge that there are many naturally occurring minerals containing radioactive and non-radioactive species very similar to the radionuclides of concern in wastes from fuel reprocessing, and that these minerals can exhibit excellent chemical durability.

In the study described here, ceramic compositions were developed for two of the nominal waste streams anticipated from the AFCI aqueous separations process. The waste forms were fabricated using three different methodologies, which vary in their proximity to equilibrium conditions, to provide insight into the stability of the phase assemblage that was formed. The ceramic materials were then characterized to determine the type and morphology of the phases present, the bulk chemical composition, the distribution of the waste species among the various phases, chemical durability, and resistance to ion beam radiation damage. These initial results led to the development of a second phase of compositions designed to improve waste loading and eliminate excess ceramic components. The Phase II materials were further characterized, and recommendations for follow-on work are provided.

2. EXPERIMENTAL PROCEDURE

2.1. Projected Waste Stream Compositions

The waste streams that formed the basis of the development testing completed in 2009 continue to be of interest for the 2010 studies, and are given in Table 2-1. The CS/LN composition is the result of a combination of the Cs/Sr separated stream and the Trivalent Actinide - Lanthanide Separation by Phosphorous reagent Extraction from Aqueous Komplexes (TALSPEAK) waste stream consisting of lanthanide fission products.[10] The CS/LN/TM streams are comprised of the Cs/Sr stream, the lanthanide stream, and the transition metal fission product waste stream resulting from the transuranic extraction (TRUEX) process.   The TM stream varies significantly due to uncertainty in volatile-oxidation separations efficiency for noble metals, partitioning of noble metals to undissolved solids, Mo and Zr concentrations in the undissolved solids and amount of Zr-molybdates precipitated during processing. Therefore, two variants of the CS/LN/TM combined waste streams have been used in waste form studies. The CS/LN/TM High Mo waste stream variant[10] has a high molybdenum concentration with relatively low noble metal concentrations, while the CS/LN/TM High NM variant[11] has high noble metal concentrations and less Mo. The CS/LN waste stream and the CS/LN/TM High Mo waste stream were selected as the focus of the current work since Mo is expected to present difficulties in phase formation in the ceramic. Furthermore, although the noble metals in the CS/LN/TM High NM waste stream are expected to exhibit low solubility, it is expected that the noble metals will remain relatively inert within the ceramic matrix.

Table 2-1. Projected Waste Stream Compositions (wt %) for Waste Form Development.[10, 11]

Oxide	CS/LN	CS/LN/TM High Mo	CS/LN/TM High NM
SeO_2	-	0.29	0.32
Br	-	0.08	0.09
Rb_2O	2.22	1.50	1.63
SrO	5.14	3.49	3.77
Y_2O_3	0.49	2.23	2.41
ZrO_2	-	10.60	3.33
MoO_3	-	13.88	3.00
RuO_2	-	0.70	6.20
Rh_2O_3	-	0.28	1.21
PdO	-	0.06	5.73
Ag_2O	-	0.40	0.43
CdO	-	0.39	0.43
In_2O_3	-	0.01	0.01
SnO_2	-	0.25	0.27
Sb_2O_3	-	0.04	0.05
TeO_2	-	2.33	2.52
Cs_2O	15.08	10.22	11.05
BaO	11.55	7.83	8.47
La_2O_3	8.21	5.62	6.08
Ce_2O_3	15.28	11.01	11.91
Pr_2O_3	7.51	5.14	5.56
Nd_2O_3	27.11	18.56	20.07
Pm_2O_3	0.08	0.06	0.06
Sm_2O_3	5.58	3.82	4.13
Eu_2O_3	0.89	0.61	0.66
Gd_2O_3	0.84	0.57	0.62
Tb_2O_3	0.02	0.01	0.01

2.2. Design of Ceramic Host Systems

Ceramic host systems for this study were selected based on the objectives of forming durable titanate and aluminate phases, using a minimum of additives to form the desired phases (i.e., achieving high waste loadings), and fabrication from a melt. Target compositions for the CS/LN waste form are given in Table 2-2. The only additives used were Al_2O_3 and TiO_2, with targeted waste loadings of 50-52 wt %. The alkali and alkaline earth elements in the waste were anticipated to partition to aluminotitanate phases approximating hollandite or $(Ba,Cs,Rb)(Al,Ti)_2Ti_6O_{16}$. The lanthanides were anticipated to partition to aluminate perovskites ($LnAlO_3$) and the strontium to a titanate perovskite ($SrTiO_3$).

Table 2-2. Target Compositions for the Phase I CS/LN Ceramic Waste Forms.

Component	CS/LN-03	CS/LN-04	CS/LN-05
Waste	52	50	50
Al_2O_3	18	15	20
TiO_2	30	35	30

The target phases for the CS/LN/TM High Mo waste stream were similar to those for the CS/LN waste stream – hollandite, Ln-Al perovskites, and $(Sr,Cd)TiO_3$ perovskites – with the addition of CaO to

produce powellite (Ca,Sr,Cd)MoO_4, calzirite (CaZrO_3), and other minor oxides. Slightly higher waste loadings of 55-60 wt % were targeted for this waste stream. The target compositions for the CS/LN/TM High Mo waste forms are given in Table 2-3.

Table 2-3. Target Compositions (wt %) for the Phase I CS/LN/TM High Mo Ceramic Waste Forms.

Component	CS/LN/TM High Mo-02	CS/LN/TM High Mo-03	CS/LN/TM High Mo-04	CS/LN/TM High Mo-05
Waste	60	55	55	55
Al_2O_3	14	15	15	15
TiO_2	21	25	23	20
CaO	5	5	7	10

As will be shown in the following sections, the first set of ceramic waste forms (Phase I) were found to contain a significant excess of Al_2O_3 after sintering. Therefore, a series of Phase II compositions were developed with reduced Al_2O_3 concentrations, calculated to provide only enough Al_2O_3 to form the desired phases incorporating the alkaline and alkaline earth components of the wastes. The Phase II compositions are given in Table 2-4.

Table 2-4. Target Compositions (wt %) for the Phase II CS/LN and CS/LN/TM High Mo Ceramic Waste Forms.

Component	CS/LN-06	CS/LN-08	CS/LN-09
Waste	50.0	55.0	60.0
Al_2O_3	4.0	7.3	8.0
TiO_2	46.0	37.7	32.0
Component	CS/LN/TM High Mo-06	CS/LN/TM High Mo-08	CS/LN/TM High Mo-09
Waste	55.0	60.0	65.0
Al_2O_3	3.0	5.4	5.9
TiO_2	35.0	27.6	19.1
CaO	7.0	7.0	10.0

2.3. Fabrication Methods

Simulated waste material and the ceramic forming additives were blended in the appropriate ratios via ball milling. Three different fabrication methods were used to densify the ceramic waste forms, including melting and crystallizing, cold pressing and sintering for extended periods, and rapid heating under pressure via spark plasma sintering. The intent was to provide insight into the phase assemblage that is formed at varying proximity to equilibrium conditions. These fabrication steps are described in further detail below.

2.3.1. Simulated Waste and Additives

Two large batches of simulated waste material (the CS/LN and CS/LN/TM High Mo compositions in Table 2-1) were prepared from proper amounts of reagent grade metal oxides and carbonates. Five of the very minor components, including Br, In_2O_3, Pm_2O_3, Sb_2O_3, and Tb_2O_3, were omitted from the simulated waste due to their very low projected concentrations. The powders were ball milled in a mixture of 50% ethyl alcohol and 50% deionized water inside polyethylene jars with flat-ended cylindrical alumina media

for 15 minutes. The blended powders were dried overnight at 70 °C. Smaller batches of each of the waste forms were then prepared by combining a portion of the simulated waste material with the appropriate amounts of reagent grade Al_2O_3 and TiO_2 (the CS/LN compositions in Table 2-2) or Al_2O_3, TiO_2 and CaO (the CS/LN/TM High Mo compositions in Table 2-3). The powders were again ball milled in an ethyl alcohol and water mixture and dried to produce batch material for each of the sintering methods.

2.3.2.   Melting and Crystallizing

Samples of each of the ceramic materials were melted in an electric resistance heated furnace to simulate melter production. The blended and dried powders were placed into Pt/Rh alloy crucibles and melted at 1500 °C for 1 hour. Power to the furnace was then turned off with the crucibles remaining inside to cool slowly (furnace cooling) to roughly approximate the slow cooling conditions experienced by a waste form poured from a melter into a canister. The temperature of the furnace during cooling was recorded, and the data are plotted in Figure 2-1. The temperature of the furnace fell below 200 °C after 6.5 hours of cooling. The crucibles were removed from the furnace once cooled and photographed to document the degree of melting that occurred for each composition.
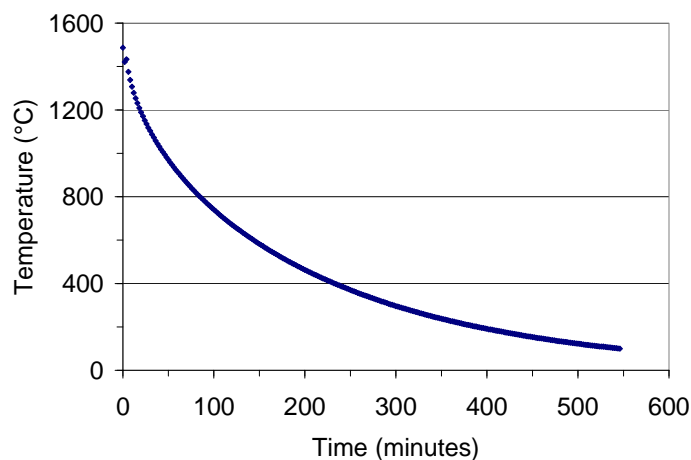
Figure 2-1. Furnace cooling profile.

2.3.3.   Cold Pressing and Sintering for Extended Periods

Sintering of pellets for longer periods was used to approximate equilibrium conditions and allow the more stable phases to form within each composition. The blended and dried powders were cold pressed into pellets using a steel die and uniaxial hydraulic press. Thermal analysis, conducted as a screening tool for crystallization and melting point determination, indicated that a majority of the compositions displayed initial melting point endotherms in the range of 1280-1300 °C. The pellets were then sintered in an electric resistance heated furnace at 1200 °C in air for 25 hours and furnace cooled.

2.3.4.   Spark Plasma Sintering

Spark plasma sintering (SPS) is a powder densification process similar to hot pressing, except that heating occurs directly by passing a pulsed DC current through the die and powder rather than using resistive heating elements. This allows for very rapid heating of the powder and enhanced sintering due to high localized temperatures at particle interfaces, electric field assisted diffusion, and plastic deformation.

Materials can typically be sintered via SPS at temperatures much lower than those of other sintering techniques and in much shorter times. SPS was explored for the ceramic waste forms to gauge the impacts of sintering at conditions far from equilibrium on the resulting phase assemblages.

One sample of the CS/LN-03 composition and one sample of the CS/LN/TM High Mo-03 composition were sintered via SPS. The experiments were carried out using a SPS Model 25-10.[a] Approximately 2 g of the sample powder were placed in a graphite die of approximately 20 mm diameter lined with graphite foil. The loaded die set was placed into the SPS chamber and a pressure of 3 MPa was applied. The chamber was evacuated and then backfilled with argon to 9.4×10^{-4} Torr. The sample was then heated from room temperature to 600 °C at a rate of 150 °C per minute using a DC pulse duration of 25 ms on and 5 ms off. The pressure was increased from 3 to 10 MPa during this time. The sample was held at 600 °C for 15 seconds. Heating then continued at 100 °C per minute to 1300 °C, with the pressure being increased from 10 to 100 MPa during this time. The sample was held at 1300 °C and 100 MPa for 15 minutes. The pressure was then relieved and the current was turned off to allow the sample to cool. It was noted, by using a displacement transducer mounted on the hydraulic ram, that densification of the samples began at approximately 900 °C and mostly ceased at approximately 1010 °C. Further densification was noted during the hold period at 1300 °C. After cooling, the samples were removed from the graphite die set and returned to SRNL for characterization. Some of the graphite foil remained adhered to the samples after removal from the die.

2.4. Characterization of Crystalline Waste Forms

2.4.1. X-ray Diffraction

Representative samples of each ceramic waste form were submitted to SRNL Analytical Development (AD) for X-ray diffraction (XRD) analysis. Samples were run under conditions providing a detection limit of approximately 0.5 vol %. That is, if crystals were present at 0.5 vol % or greater, the diffractometer would allow a qualitative determination of the type of crystalline phases present. Samples were ground prior to analysis. In some cases, the surfaces of unground samples were first analyzed to determine any differences between surface and bulk phase assemblage.

2.4.2. Chemical Compositions

Representative samples of select compositions were characterized to confirm that the as-fabricated ceramics met the target compositions. A lithium-metaborate fusion was used to dissolve the samples. The resulting solutions were analyzed by Inductively Coupled Plasma – Atomic Emission Spectroscopy (ICP-AES). Two measurements were taken for each element of interest, and the average of these two measurements was reported as the measured value. Inductively Coupled Plasma – Mass Spectroscopy (ICP-MS) was used to measure the concentrations of Cs, Pd, Rh, and Ru. Only one measurement was performed for each of these elements.

2.4.3. Electron Microscopy and Elemental Analysis

Scanning Electron Microscopy (SEM) and Energy Dispersive Spectroscopy (EDS) analyses were performed at LANL on select samples. Specimens were cut, ground, and polished with alumina lapping films to produce a flat surface for imaging and analysis. All of the samples were final polished using 40 nm colloidal silica slurry[b] to remove mechanical polishing damage. Secondary electron and

---

[a] SPS performed at Thermal Technology LLC, Santa Rosa, CA 95403.
[b] Syton HT50, DuPont AirProducts NanoMaterials L.L.C, Tempe, AZ.

backscattered electron imaging were used to identify grain size and morphology, as well as general homogeneity of the specimen. EDS elemental mapping was used to identify partitioning of the waste elements among the various phases.

2.4.4. Chemical Durability

The ASTM C1285 Product Consistency Test (PCT) Method B was used to provide a preliminary measure of the chemical durability of the ceramic waste forms. This test was used to provide preliminary insight into the rate of leaching of the waste elements from the ceramic materials due to the relative ease of performing the experiments and the relatively short time period (7 days) needed for testing, although it may not be the optimal method.

The PCT Method-B was performed on select samples of the Phase I and Phase II compositions. Also included were samples of the Approved Reference Material (ARM) glass. Samples were ground, washed, and prepared according to the ASTM procedure. Ten milliliters of Type-I ASTM water were added to 1.0 g of the ground sample in stainless steel vessels. The vessels were closed, sealed, and placed in an oven at 90 °C for 7 days. Once cooled, the resulting solutions were filtered and acidified, then analyzed by ICP-AES. Normalized release rates were calculated based on the measured compositions using the average of the common logarithms of the leachate concentrations. Note that the small amount of material available for each composition dictated that the testing had to be performed with either single samples or duplicates. The number of replicates (if any) for each composition will be discussed in the results.

2.4.5. Ion Beam Irradiation

Preliminary evaluations of the radiation damage tolerance of the ceramic waste forms were undertaken by subjecting select samples to alpha particle irradiation at LANL. A 5 MeV He ion beam with a fluence of $1x10^{17}$ ions/cm^2 was used with the samples (polished as described earlier) at room temperature. The samples were evaluated by SEM and XRD before and after irradiation to identify any microstructural changes induced by alpha bombardment.

3. RESULTS AND DISCUSSION

3.1. Fabrication of Ceramic Waste Forms

Photographs of the Phase I CS/LN waste forms fabricated from 1500 °C melts are shown in Figure 3-1. Each of the three compositions appeared to have melted completely, with some void spaces after cooling and a mottled appearance that may be indicative of their multiphase composition. Photographs of the Phase I CS/LN/TM High Mo Waste Forms are shown in Figure 3-2. Only the Cs/LN/TM High Mo-03 composition appeared to melt completely in this group. The CS/LN/TM High Mo-02 and CS/LN/TM High Mo-04 compositions appeared to have melted partially, with most of the porosity eliminated. The CS/LN/TM High Mo-05 appeared to have densified to some degree, but little or no melting occurred. The higher concentration of TiO_2 in the CS/LN/TM High Mo-03 composition appears to have aided in melting at 1500 °C. When the TiO_2 concentration was reduced either to add more of the waste oxides (CS/LN/TM High Mo-02) or to add more CaO (CS/LN/TM High Mo-04 and -05), the temperature required for complete melting increased.

(CS/LN-03)   (CS/LN-04)   (CS/LN-05)
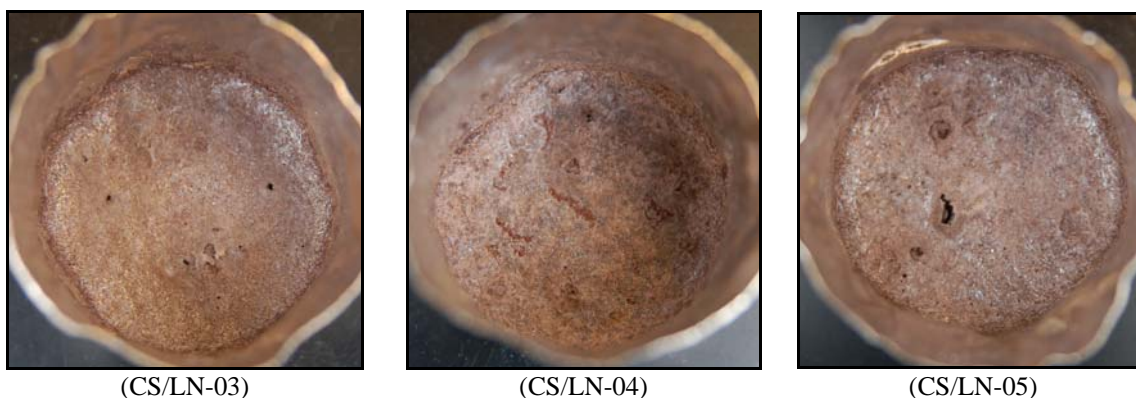
**Figure 3-1. Photographs of the Phase I CS/LN Waste Forms
after Melting and Crystallizing.**

(CS/LN/TM High Mo-02)   (Cs/LN/TM High Mo-03)

(CS/LN/TM High Mo-04)   (CS/LN/TM High Mo-05)
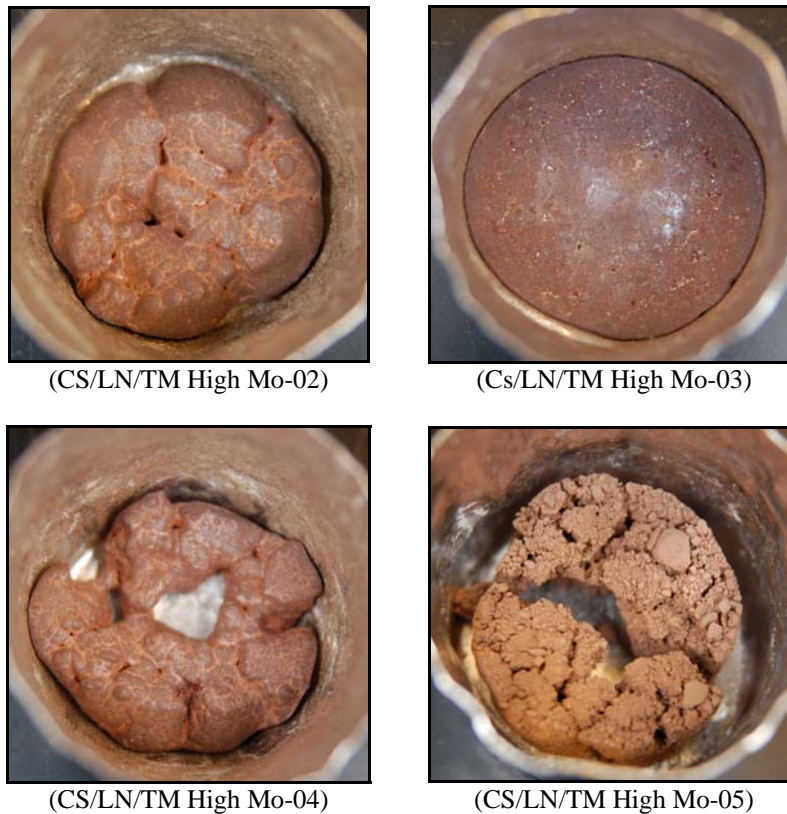
**Figure 3-2. Photographs of the Phase I CS/LN/TM High Mo
Waste Forms after Melting and Crystallizing.**

Photographs of the Phase II CS/LN waste forms fabricated from 1500 °C melts are shown in Figure 3-3. The CS/LN-06 and -08 compositions appeared to have melted completely. The CS/LN-09 composition, which has a higher concentration of waste oxides and Al_2O_3 in place of TiO_2, appears to have become too refractory to melt completely at 1500 °C. Photographs of the Phase II CS/LN/TM High Mo Waste Forms are shown in Figure 3-4. None of these compositions melted completely at 1500 °C, although the CS/LN/TM High Mo-06 composition appeared to have melted partially with most of the porosity eliminated. As the waste oxides, Al_2O_3, and CaO concentrations were increased in the Phase II series (and TiO_2 concentrations were subsequently decreased), the compositions appear to have become more refractory.

| (CS/LN-06) | (CS/LN-08) | (CS/LN-09) |
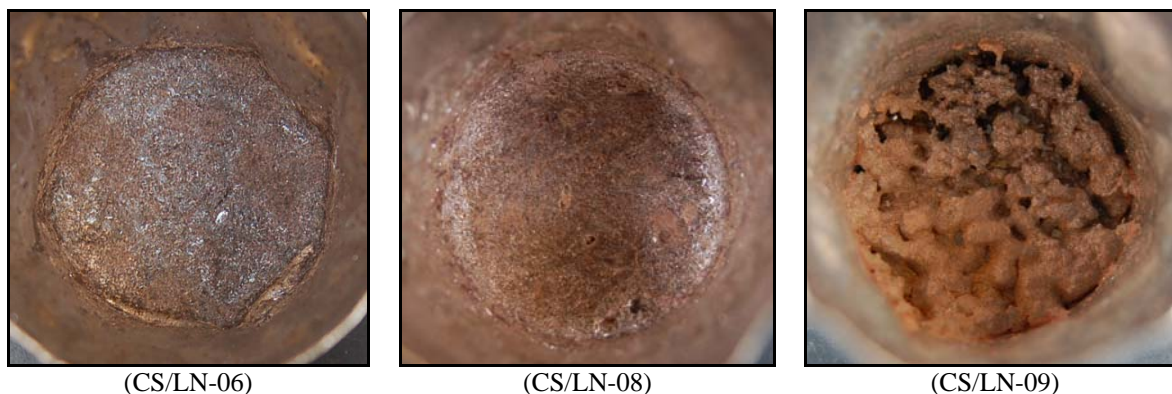
**Figure 3-3. Photographs of the Phase II CS/LN Waste Forms
after Melting and Crystallizing.**

| (CS/LN/TM High Mo-06) | (CS/LN/TM High Mo-08) | (CS/LN/TM High Mo-09) |

**Figure 3-4. Photographs of the Phase II CS/LN/TM High Mo
Waste Forms after Melting and Crystallizing.**

The pellets fabricated by free sintering at 1200 °C were not fully densified. The pellets fabricated by SPS appeared to be denser, although likely still contained porosity as judged by their low handling strength. Some of the graphite foil used to line the SPS die remained adhered to the pellets after sintering. Density of the pellets was not measured due to the small amount of sample material available.

3.2. Chemical Compositions

The results of the chemical composition measurements of the Phase I, CS/LN waste forms fabricated by melting and crystallizing are given in Table 3-1. The target compositions are included for comparison. In general, most of the components are present at concentrations close to their targeted values. The Cs_2O concentrations are about 20-30% below their target values, which is likely due to volatilization during melting. There may have also been some volatilization of La_2O_3. Note that some SiO_2 was measured in the samples, while no silica was intentionally added. This is likely due to impurities in the reagent powders used as batch material, or may be caused by inhomogeneity in the material.

The results of the chemical composition measurements of the Phase I, CS/LN/TM High Mo waste forms fabricated by melting and crystallizing are given in Table 3-2. The target compositions are again included

for comparison. Similar to the CS/LN waste forms, most of the components of the CS/LN/TM High Mo waste forms are present at concentrations close to their targeted values. Volatilization of Cs_2O is again apparent. The concentrations of Cs_2O in these samples are about 50% below their targeted values. Approximately 30-40% of the MoO_3 appears to have volatilized. Concentrations of some of the minor components, including Ag_2O, CdO, Rb_2O and Rh_2O_3 are below their target values, again likely due to volatilization. More severe volatilization appears to have occurred for RuO_2, SeO_2 and TeO_2. However, the target concentrations of several of these components were quite low, which may have led to minor issues with representative sampling. Note that the La_2O_3 concentrations in these compositions are much closer to their targeted values than those of the CS/LN waste forms. A small amount of SiO_2 is again present.

Table 3-1. Target and Measured Compositions (wt %) of the Phase I CS/LN Waste Forms Fabricated by Melting and Crystallizing.

Oxide	CS/LN-03		CS/LN-04		CS/LN-05	
	Target	Measured	Target	Measured	Target	Measured
Al_2O_3	18.00	19.66	15.00	16.01	20.00	20.41
BaO	6.01	5.73	5.78	5.68	5.78	5.98
Ce_2O_3	7.95	7.09	7.65	7.11	7.65	7.14
Cs_2O	7.85	6.41	7.55	5.59	7.55	6.39
Eu_2O_3	0.46	0.36	0.45	0.37	0.45	0.37
Gd_2O_3	0.44	0.40	0.42	0.40	0.42	0.41
La_2O_3	4.27	3.57	4.11	3.59	4.11	3.51
Nd_2O_3	14.11	13.60	13.57	13.85	13.57	13.59
Pr_2O_3	3.91	3.59	3.76	3.66	3.76	3.58
Rb_2O	1.16	1.00	1.11	0.91	1.11	1.00
SiO_2	0.00	0.38	0.00	0.43	0.00	0.29
Sm_2O_3	2.90	2.73	2.79	2.77	2.79	2.74
SrO	2.68	2.70	2.57	2.74	2.57	2.64
TiO_2	30.00	30.69	35.00	33.94	30.00	30.00
Y_2O_3	0.26	0.21	0.25	0.21	0.25	0.22
Total	100.00	98.11	100.00	97.27	100.00	98.27

Table 3-2. Target and Measured Compositions (wt %) of the Phase I CS/LN/TM High Mo Waste Forms Fabricated by Melting and Crystallizing.

Oxide	CS/LN/TM High Mo-02		CS/LN/TM High Mo-03		CS/LN/TM High Mo-04		CS/LN/TM High Mo-05	
	Target	Measured	Target	Measured	Target	Measured	Target	Measured
Ag_2O	0.24	0.15	0.22	0.14	0.22	0.13	0.22	0.10
Al_2O_3	14.00	15.49	15.00	16.91	15.00	16.58	15.00	16.44
BaO	4.71	4.60	4.32	4.12	4.32	4.20	4.32	4.61
CaO	5.00	5.49	5.00	5.59	7.00	7.70	10.00	10.75
CdO	0.23	0.11	0.21	0.11	0.21	0.08	0.21	0.02
Ce_2O_3	6.62	6.87	6.07	6.26	6.07	6.18	6.07	6.08
Cs_2O	6.15	3.50	5.63	2.72	5.63	3.02	5.63	3.13
Eu_2O_3	0.37	0.31	0.34	0.29	0.34	0.28	0.34	0.27
Gd_2O_3	0.34	0.33	0.31	0.32	0.31	0.31	0.31	0.30
La_2O_3	3.38	3.31	3.10	3.01	3.10	2.98	3.10	2.95
MoO_3	8.35	6.02	7.65	4.71	7.65	5.23	7.65	6.21
Nd_2O_3	11.16	12.71	10.23	11.66	10.23	11.47	10.23	11.31
PdO	0.04	0.04	0.03	0.04	0.03	0.04	0.03	0.04
Pr_2O_3	3.09	3.35	2.83	3.03	2.83	3.03	2.83	2.99
Rb_2O	0.90	0.77	0.83	0.58	0.83	0.66	0.83	0.75
Rh_2O_3	0.17	0.05	0.15	0.05	0.15	0.04	0.15	0.05
RuO_2	0.42	0.04	0.39	0.03	0.39	0.02	0.39	0.01
SeO_2	0.17	0.00	0.16	0.00	0.16	0.00	0.16	0.00
SiO_2	0.00	0.42	0.00	0.65	0.00	0.52	0.00	0.52
Sm_2O_3	2.30	2.49	2.11	2.28	2.11	2.25	2.11	2.23
SnO_2	0.15	0.13	0.14	0.12	0.14	0.12	0.14	0.11
SrO	2.10	2.46	1.92	2.22	1.92	2.24	1.92	2.26
TeO_2	1.40	0.48	1.28	0.52	1.28	0.37	1.28	0.04
TiO_2	21.00	20.81	25.00	25.16	23.00	22.77	20.00	19.54
Y_2O_3	1.34	1.41	1.23	1.33	1.23	1.30	1.23	1.29
ZrO_2	6.37	6.30	5.84	5.98	5.84	5.93	5.84	5.82
Total	100.00	97.65	100.00	97.82	100.00	97.46	100.00	97.84

Chemical composition results for the Phase II CS/LN waste forms and their target compositions are given in Table 3-3. The measurements for Cs_2O in the Phase II compositions had not been completed at the time of this report. These data will be reported in FY2011. Most of the components are present in concentrations close to their targeted values. A minor amount of volatilization appears to have occurred for La_2O_3. The measured concentration of TiO_2 in composition CS/LN-06 is below the target, which may be due to misrepresentative sampling or an inhomogeneous melt.

Chemical composition results for the Phase II CS/LN/TM High Mo compositions, again without Cs_2O, are given along with their target values in Table 3-4. As with the other samples, most of the components are present at concentrations close to their targeted values. The CaO values seem unusually high. This high value (as well as high values for some of the other components) could indicate that a large amount of the Cs_2O volatilized during melting. This will be confirmed via ICP-MS measurements, which are in progress. The components CdO, MoO_3, Rb_2O, Rh_2O_3, RuO_2, SeO_2, and TeO_2 appear to have volatilized to varying degrees during melting, although the target concentrations of some of these components were quite small.

Table 3-3. Target and Measured Compositions (wt %) of the Phase II CS/LN Waste Forms Fabricated by Melting and Crystallizing.

Oxide	CS/LN-06		CS/LN-08		CS/LN-09	
	Target	Measured	Target	Measured	Target	Measured
Al_2O_3	4.00	4.38	7.34	8.11	8.01	8.65
BaO	5.78	5.41	6.36	5.82	6.94	6.25
Ce_2O_3	7.65	7.26	8.41	7.80	9.18	8.55
Eu_2O_3	0.45	0.37	0.49	0.41	0.53	0.44
Gd_2O_3	0.42	0.37	0.46	0.40	0.50	0.44
La_2O_3	4.11	3.48	4.52	3.79	4.93	4.17
Nd_2O_3	13.57	12.83	14.93	14.00	16.28	15.45
Pr_2O_3	3.76	3.42	4.13	3.75	4.51	4.14
Rb_2O	1.11	1.19	1.22	1.20	1.33	1.48
Sm_2O_3	2.79	2.27	3.07	2.50	3.35	2.72
SrO	2.57	2.68	2.83	2.89	3.09	3.18
TiO_2	46.00	42.63	37.66	36.71	31.99	31.45
Y_2O_3	0.25	0.20	0.27	0.21	0.29	0.22

Table 3-4. Target and Measured Compositions (wt %) of the Phase II CS/LN/TM High Mo Waste Forms Fabricated by Melting and Crystallizing.

Oxide	CS/LN/TM High Mo-06		CS/LN/TM High Mo-08		CS/LN/TM High Mo-09	
	Target	Measured	Target	Measured	Target	Measured
Ag_2O	0.22	0.17	0.24	0.17	0.26	0.09
Al_2O_3	3.00	3.69	5.43	6.38	5.88	6.82
BaO	4.32	4.61	4.71	4.90	5.10	5.33
CaO	7.00	7.99	7.00	8.30	10.00	11.22
CdO	0.21	0.03	0.23	0.00	0.25	0.00
Ce_2O_3	6.07	6.73	6.62	7.30	7.17	7.80
Eu_2O_3	0.34	0.33	0.37	0.36	0.40	0.38
Gd_2O_3	0.31	0.32	0.34	0.35	0.37	0.37
La_2O_3	3.10	3.14	3.38	3.39	3.66	3.58
MoO_3	7.65	5.12	8.35	5.70	9.04	7.37
Nd_2O_3	10.23	11.62	11.16	12.48	12.09	13.30
Pr_2O_3	2.83	3.07	3.09	3.33	3.35	3.59
Rb_2O	0.83	0.56	0.90	0.65	0.98	0.80
Rh_2O_3	0.15	0.00	0.17	0.00	0.18	0.00
RuO_2	0.39	0.00	0.42	0.00	0.46	0.00
SeO_2	0.16	0.00	0.17	0.00	0.19	0.00
Sm_2O_3	2.11	2.06	2.30	2.23	2.49	2.38
SnO_2	0.14	0.11	0.15	0.13	0.16	0.13
SrO	1.92	2.32	2.10	2.56	2.27	2.72
TeO_2	1.28	0.13	1.40	0.04	1.52	0.04
TiO_2	35.00	34.95	27.57	28.86	19.12	19.69
Y_2O_3	1.23	1.07	1.34	1.18	1.45	1.26
ZrO_2	5.84	6.13	6.37	6.78	6.91	7.29

3.3.   Electron Microscopy and Elemental Analysis

Samples of compositions CS/LN-05 and CS/LN/TM High Mo-02 fabricated by melting and crystallizing, and composition CS/LN-09 fabricated by pressing and sintering were sent to LANL for SEM/EDS analyses. A backscattered electron micrograph of composition CS/LN-05 is shown in Figure 3-5. The differences in contrast indicate at least four crystalline phases, with varying grain sizes and morphology. Porosity is visible as the black area at the left of the micrograph. The more angular black areas may indicate grain pullout during polishing.
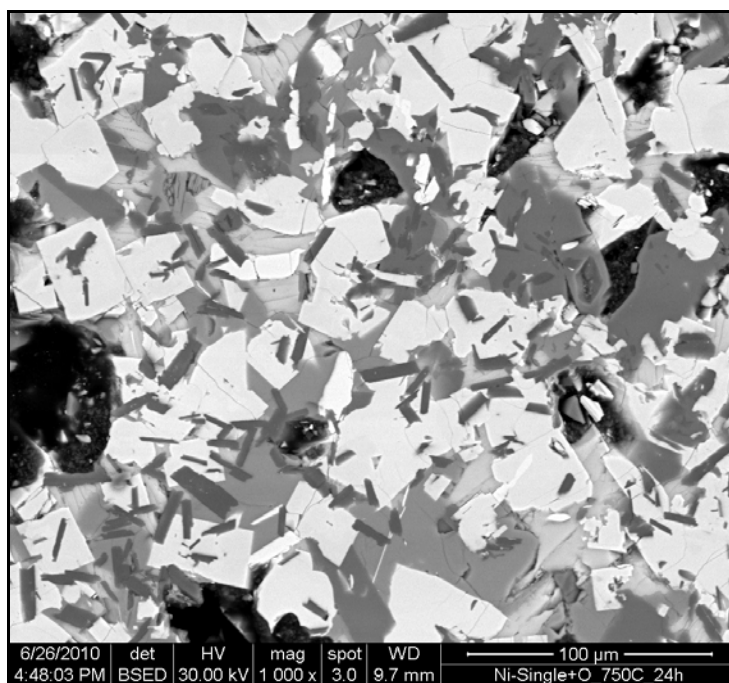
Figure 3-5. Backscattered Electron Micrograph of a Polished Surface of Composition CS/LN-05 Fabricated by Melting and Crystallizing.

The results of EDS elemental mapping for this sample are shown in Figure 3-6. Observations of these maps show that:

- Unreacted Al_2O_3 is readily apparent as high aspect ration, or needle-like grains.
- Ba appears to partition mainly to a titanate phase, but is present in all of the phases except for the unreacted Al_2O_3.
- Ce appears to partition most strongly to a different titanate phase, with additional Ba and Nd.
- Cs and La appear to partition to the same phase, although La is also distributed in other phases.
- Nd and Pr appear to partition to the same phases.
- O is dispersed throughout the material as expected, although higher concentrations appear with Al.
- Rb and Sr are distributed fairly uniformly, although some of the Sr appears to partition to the phase containing Nd and Pr.
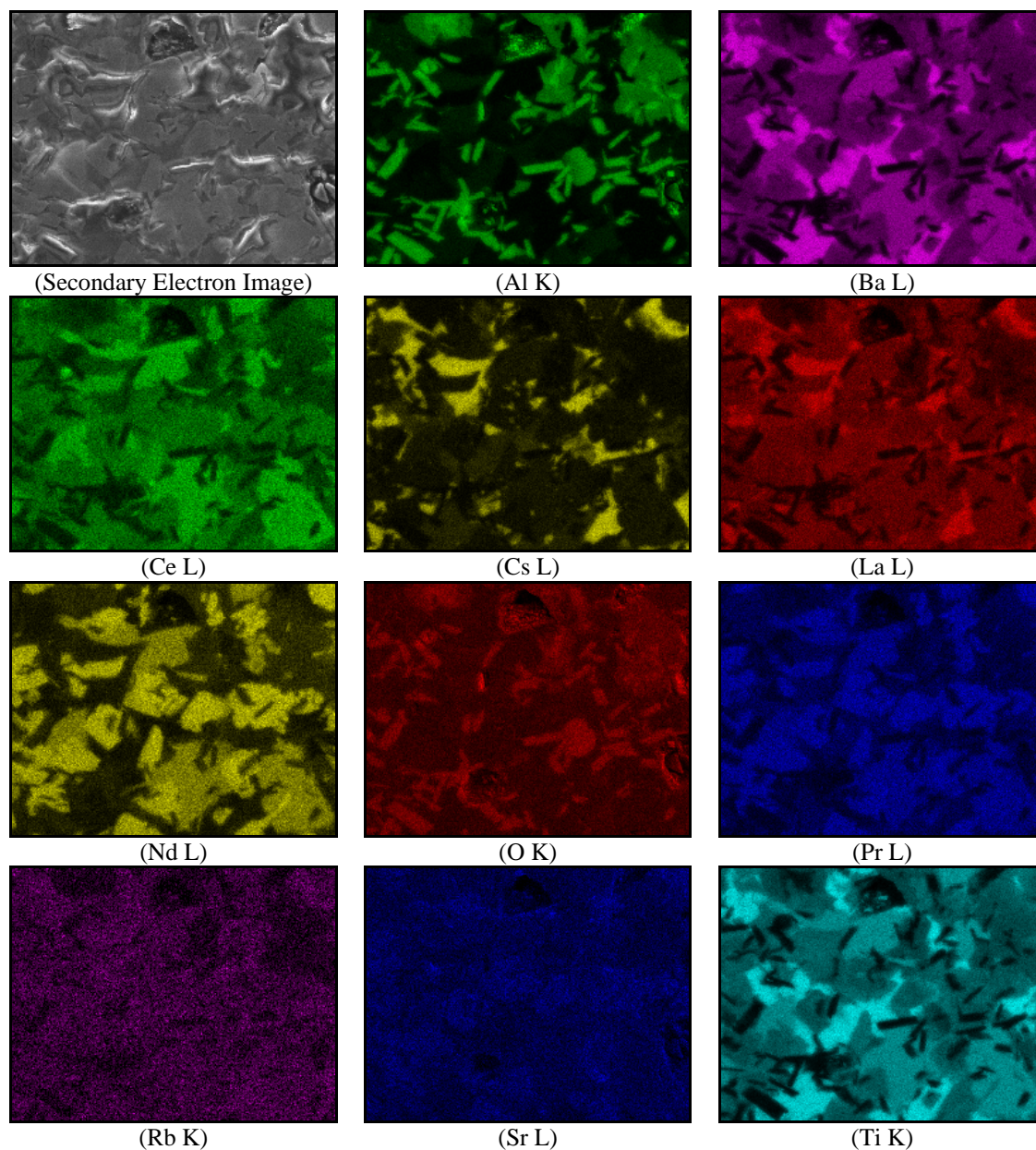
Figure 3-6. EDS Mapping for Select Elements in Composition CS/LN-05 Fabricated by Melting and Crystallizing. The Element and Emission Line Are Given for Each Image.

A backscattered electron micrograph of composition CS/LN/TM High Mo-02 is shown in Figure 3-7. The lower density of this material made it difficult to obtain a good polished surface for analysis. However, the backscattered image shows at least four crystalline phases present based on differences in contrast. The phases vary widely in grain size and morphology. The light gray phases have a considerably smaller grain size than the phases in the CS/LN-05 sample (Figure 3-5). Porosity is apparent, as well as the high aspect ratio or needle-like grains of unreacted Al_2O_3.

Figure 3-7. Backscattered Electron Micrograph of a Polished Surface of Composition CS/LN/TM High Mo-02 Fabricated by Melting and Crystallizing.
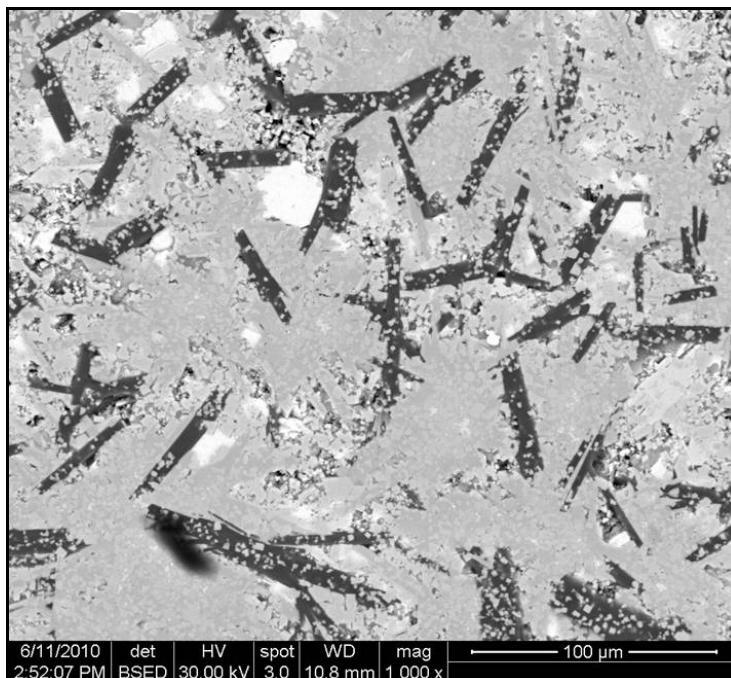
The results of EDS elemental mapping for the CS/LN/TM High Mo-02 sample are shown in Figure 3-8. Observations of these maps show that:

- Unreacted Al_2O_3 is present and Al appears to be in no other phases.
- Ba is distributed throughout the material with the exception of the Al_2O_3 grains and is most strongly associated with Ti.
- Ca is fairly well distributed, along with Pr, Sm and Sr.
- Ce and Mo appear to partition to the same phase. Ce is also distributed among the other phases.
- Cs appears to have partitioned more strongly to certain grains, but the other constituents of these grains are not clear from the EDS mapping.
- La and Nd are generally well distributed, but may partition together.
- Oxygen is dispersed throughout the material as expected, although the higher concentrations appear with Al.
- The distribution of Zr appears uneven, although none of the other elements mapped showed a similar distribution. This may be due to some type of artifact in the EDS mapping process.

**Figure 3-8. EDS Mapping for Select Elements in Composition
CS/LN/TM High Mo-02 Fabricated by Melting and Crystallizing.
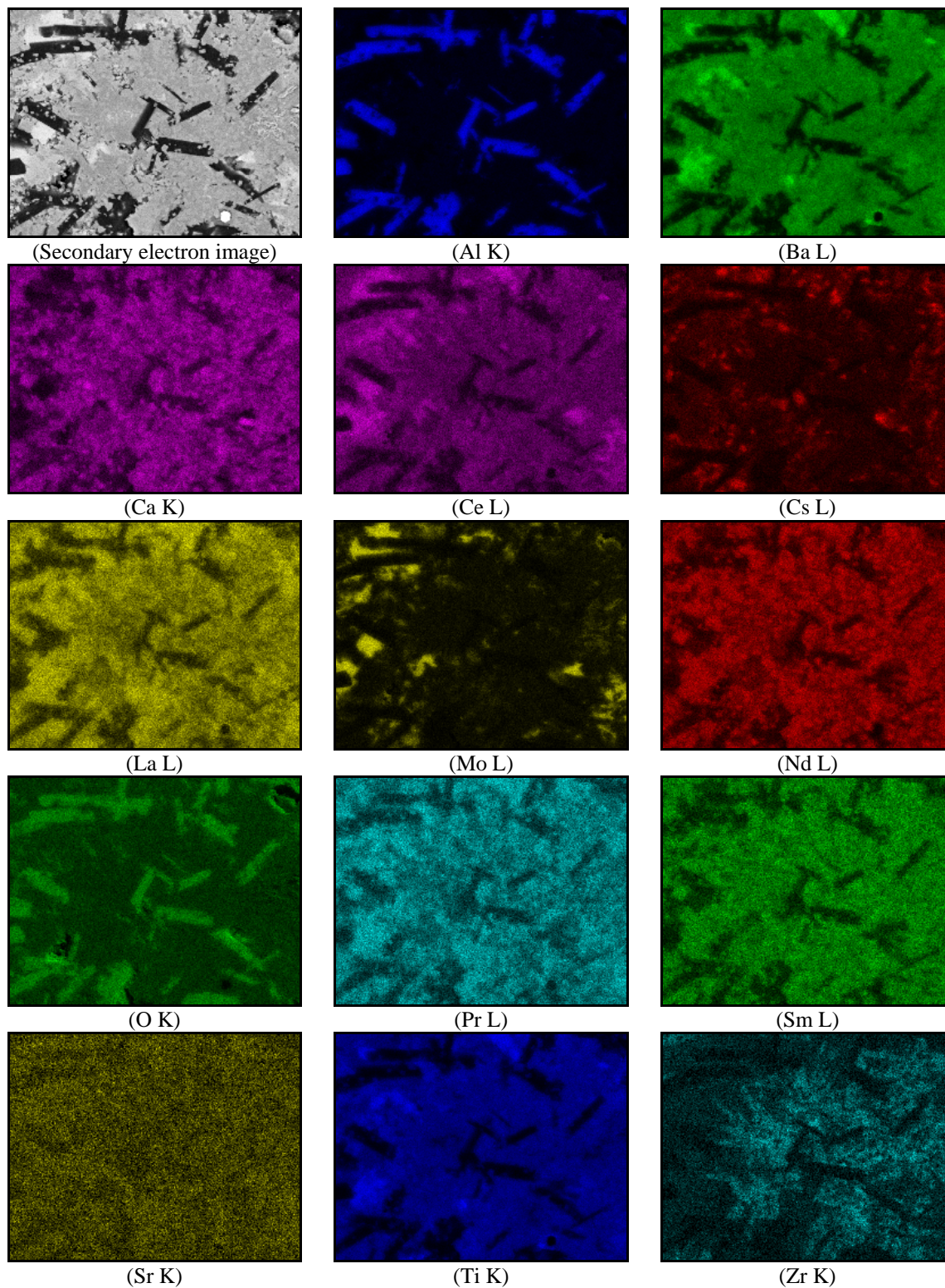The Element and Emission Line Are Given for Each Image.**

A secondary electron micrograph of composition CS/LN-09 is shown in Figure 3-9. A rough cut surface of this sample was used for analysis since its low density made polishing difficult. This Phase II composition contains a lower concentration of Al_2O_3, and does not appear to contain the elongated grains of excess Al_2O_3 seen in the previous samples. The average grain size appears to be smaller than that of the previous samples, with most grains measuring less than 10 μm in diameter. Porosity continues to be apparent. The secondary electron image does not allow for an estimate of the number of phases present based on z-contrast. However, the image suggests at least two phases based on the morphology of the grains: a phase with high aspect ratio platelet or needle-like grains, and a phase with larger diameter and smaller aspect ratio grains.

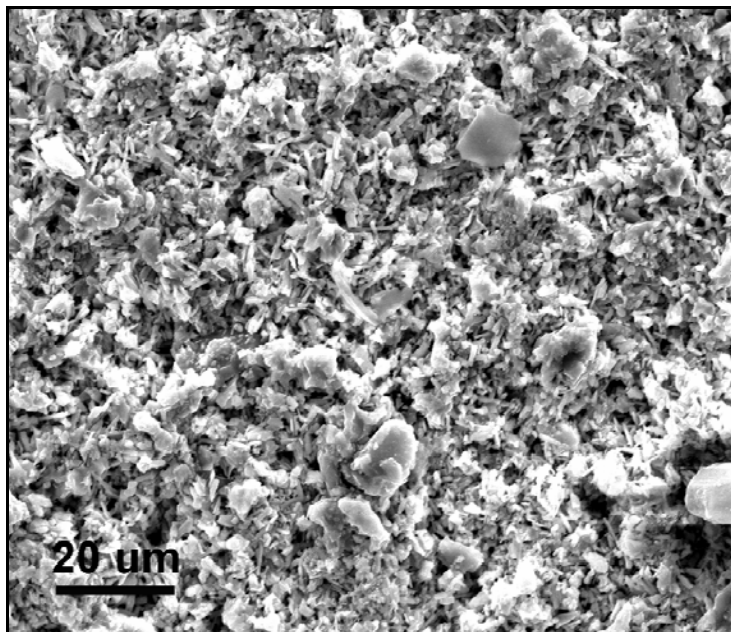**Figure 3-9. Secondary Electron Micrograph of Composition CS/LN-09
Fabricated by Pressing and Sintering.**

The results of EDS elemental mapping for the CS/LN-09 sample are shown in Figure 3-10. Observations of these maps show that:

- There are still a small number of unreacted Al_2O_3 grains present, although they are not the high aspect ratio grains seen in the previous samples. The Al_2O_3 grains do not incorporate any of the other elements analyzed.
- Ba and Ti are distributed throughout the sample except for the Al_2O_3 grains, but are in the highest concentrations together.
- Ce is distributed throughout the sample, with a few grains of higher concentration. The results for Cs are similar, although the grains with higher Cs concentrations are different from those with higher Ce concentrations.
- La, Nd, Pr, and Sm, are fairly evenly distributed throughout the sample.
- Sr appears evenly distributed among some of the phases and depleted in others.

The results of the EDS mapping will be used to aid in the identification of the crystalline phase assemblages, along with the XRD data discussed in the following section. Additional characterization of the Phase II samples will be completed in FY2011.
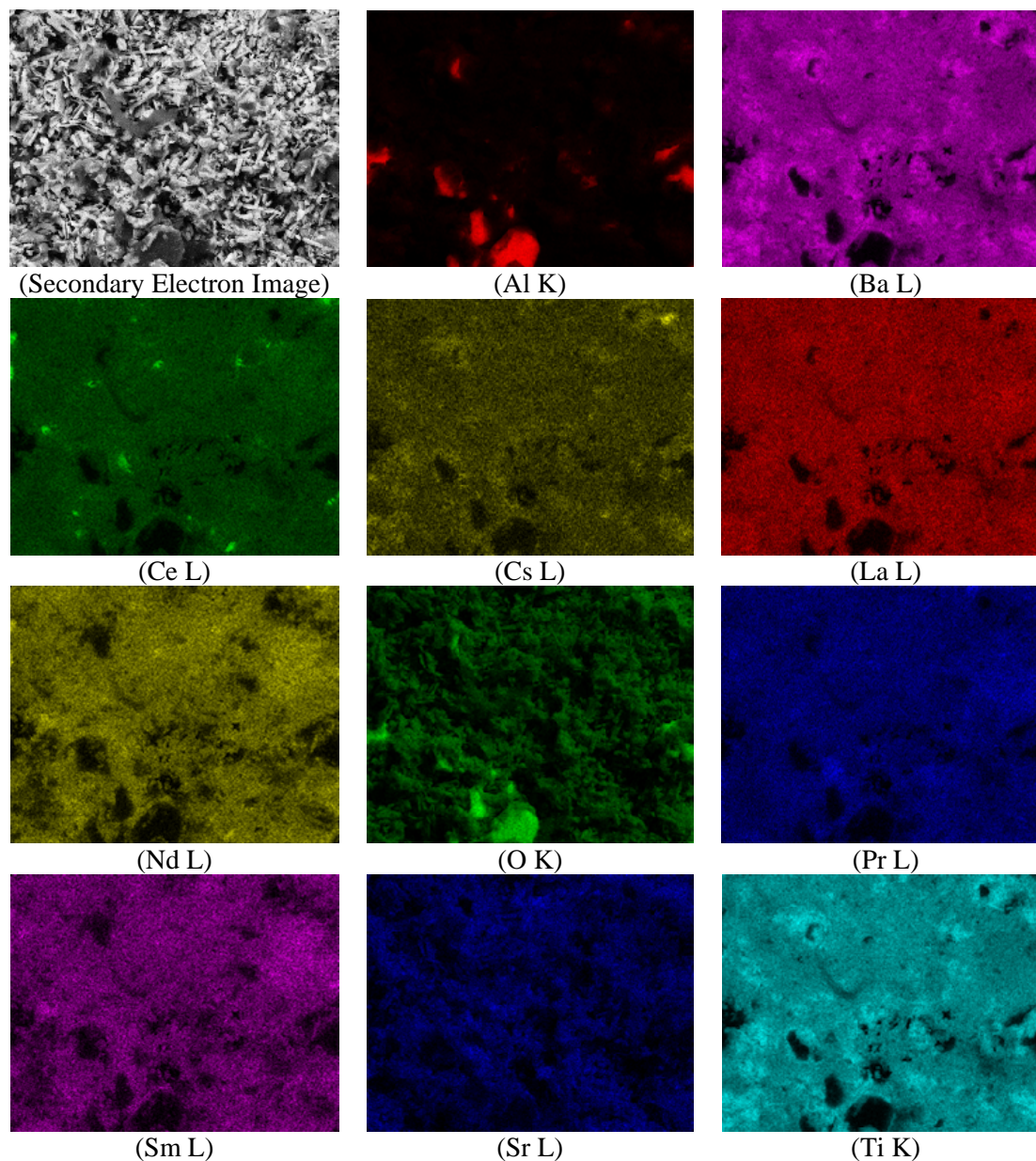
Figure 3-10. EDS Mapping for Select Elements in Composition CS/LN-09 Fabricated by Pressing and Sintering. The Element and Emission Line Are Given for Each Image.

3.4. Crystalline Phase Assemblages

XRD data for the Phase I CS/LN compositions prepared via the three fabrication methods are summarized in Table 3-5. XRD scans of the pellet surfaces and ground samples of the same material showed no texturing effects. A review of the data in Table 3-5 shows that some of the expected phases in the CS/LN system formed, while others did not. There was some dependence on the type of fabrication method used. The hollandite-type phases formed in each of the compositions as predicted. For the press and sinter method, $(Ba,Cs,Rb)Al_2Ti_5O_{14}$ was identified. The higher temperature processes produced $CsTiAlO_4$ and $(Ba,Cs)(Al_2Ti_6)O_{16}$ phases approximating hollandite. All of the methods produced the predicted $SrTiO_3$ perovskite phase, as well as $BaTiO_3$.

The $LnAlO_3$ phases predicted to host the lanthanides for the CS/LN waste composition did not form. Instead, a $Ba_4(Sr_2Sm_8)(TiO_3)_{18}$ phase was detected in all of the compositions, as well as a $Nd_2Ti_2O_7$ pyrochlore phase potentially with all the fabrication methods except for the SPS sample. The $Nd_2Ti_2O_7$ pyrochlore phase in the samples produced from melts was difficult to positively identify by XRD (as indicated by the question marks in Table 3-5), but the SEM and EDS results served to confirm the presence of this phase (see Figure 3-6). A brief review of thermodynamic data for these phases shows that the lanthanide titanate phases should indeed be more stable than the lanthanide aluminate phases originally predicted to form. The most prevalent lanthanide in the CS/LN waste stream is Nd, and the free energy of formation of $NdAlO_3$ is approximately -41 kJ/mol,[12] as compared to approximately -120 kJ/mol for $Nd_2Ti_2O_7$.[13] Although the conditions used to fabricate these compositions were likely not at equilibrium, the lower free energy of formation of $Nd_2Ti_2O_7$ is in agreement with the XRD results.

Partitioning of the waste components Ce, La, and Pr is not clear from the XRD data. Based on the EDS results (and XRD results for the Phase II compositions discussed below), it is likely that these components are present as substitutional cations in the perovskite phase. Corundum (Al_2O_3) was identified in all of the samples, indicating that an excess of Al_2O_3 was added to the compositions and remained unreacted after melting or sintering. This finding led to the reduced Al_2O_3 concentrations targeted in the Phase II compositions (see Table 2-4).

Table 3-5. Summary of XRD Data for Phase I CS/LN Waste Forms Prepared by Three Methods.

Phases	Press and Sinter			Melt and Crystallize			SPS
	CS/LN-03	CS/LN-04	CS/LN-05	CS/LN-03	CS/LN-04	CS/LN-05	CS/LN-03
$BaTiO_3/SrTiO_3$ perovskite	X	X	X	X	X	X	X
$CsTiAlO_4$ hollandite type				X	X	X	X
$(Ba,Cs)(Al_2Ti_6)O_{16}$ hollandite type							X
$(Ba,Cs,Rb)Al_2Ti_5O_{14}$ hollandite	X	X	X				
$Ba_4(Sr_2Sm_8)(TiO_3)_{18}$	X	X	X	X	X	X	X
$Nd_2Ti_2O_7$ pyrochlore	X	X	X	?	?	X (SEM/EDS)	
Unreacted Al_2O_3	X	X	X	X	X	X	X

XRD data for the Phase I CS/LN/TM High Mo compositions prepared via the three fabrication methods are summarized in Table 3-6. The results for this waste composition are similar to those of the CS/LN compositions in that some of the predicted phases formed, while others did not. No hollandite-type phases were detected in any of the CS/LN/TM High Mo waste forms. XRD scans were completed on both the sample surfaces and ground samples of the CS/LN/TM High Mo compositions fabricated by pressing and sintering. Differences between the surface scans and the ground samples indicated that there are some differences in phase assemblage (i.e., differences in volume fractions of the phases present) at the surface as compared to bulk material, but there didn't appear to be any texturing effects. The types of phases present on the surface and within the bulk were the same.

The higher concentrations of Ca and Zr in these compositions produced a $CaZrTi_2O_7$ zirconolite phase in some of the samples, corroborated by SEM/EDS data for composition CS/LN/TM High Mo-02 (see Figure 3-8). Ca and Zr in the compositions fabricated by pressing and sintering formed a $Ca_{0.15}Zr_{0.85}O_{1.65}$ phase. Similar to the CS/LN waste forms, the $LnAlO_3$ phases predicted to host the lanthanides for the CS/LN/TM High Mo waste composition did not form. Instead, $(La,Ce,Nd)CaTiO_3$-type perovskites were detected in all of the compositions. The Mo in these compositions is incorporated in $BaMoO_4$-type phases.

A $(Sm,Gd)_2Ti_2O_7$-type pyrochlore phase was detected in all the compositions produced by melting and crystallizing. The $BaTiO_3$ and $SrTiO_3$ perovskite phases were difficult to positively identify by XRD (as indicated by the question marks in Table 3-6), but the SEM and EDS results served to confirm the presence of this phase in composition CS/LN/TM High Mo-02 fabricated by melting and crystallizing (see Figure 3-8).

Partitioning of Cs is not clear from the XRD or EDS data. Pr has likely partitioned to the perovskite phase, similarly to the other lanthanide elements. Partitioning of the Zr in the CS/LN/TM High Mo-03, -04, and -05 compositions fabricated by pressing and sintering is also unclear. It may be that the zirconolite was present in these compositions at smaller volume fractions, which were difficult to identify via XRD. Corundum (Al_2O_3) was again identified in most of the samples, indicating that an excess of Al_2O_3 was added and remained unreacted after melting or sintering. Phase II compositions for the CS/LN/TM High Mo waste stream with reduced Al_2O_3 concentrations are given in Table 2-4.

Table 3-6. Summary of XRD Data for Phase I CS/LN/TM High Mo Waste Forms Prepared by Three Methods.

Phases	Press and Sinter				Melt and Crystallize				SPS
	CS/LN/TM High Mo-02	CS/LN/TM High Mo-03	CS/LN/TM High Mo-04	CS/LN/TM High Mo-05	CS/LN/TM High Mo-02	CS/LN/TM High Mo-03	CS/LN/TM High Mo-04	CS/LN/TM High Mo-05	CS/LN/TM High Mo-03
$(La,Ce,Nd)CaTiO_3$ perovskite	X	X	X	X	X	X	X	X	X
$BaMoO_4$	X	X	X	X	X	X	X	X	
$Ca_{0.15}Zr_{0.85}O_{1.65}$	X	X	X	X					
$(Sm,Gd)_2Ti_2O_7$ pyrochlore					X	X	X	X	
$CaZrTi_2O_7$ zirconolite		X			X (SEM/EDS)				X
$BaTiO_3/SrTiO_3$ perovskite	?	?	?	?	X (SEM/EDS)	?	?	?	
Unreacted Al_2O_3	X	X	X	X	X (SEM/EDS)	X	X	X	X

XRD data for the Phase II CS/LN compositions prepared via two of the fabrication methods (the Phase II compositions were not sintered by SPS) are summarized in Table 3-7. For most of the compositions fabricated by pressing and sintering, the predicted hollandite-type phases were successfully formed, as well as Ba perovskite and Nd pyrochlore phases. CS/LN-06, which had the lowest target Al_2O_3 concentration, had no unreacted Al_2O_3 detectable by XRD. Titanate phases differing from a typical hollandite stoichiometry formed in the CS/LN-08 and -09 compositions, but may have similar structures.

For most of the Phase II CS/LN compositions fabricated by melting and crystallizing, hollandite-type and pyrochlore phases again formed. No perovskites or unreacted Al_2O_3 were detected in these samples via XRD. However, the EDS data (Figure 3-10) show unreacted Al_2O_3 in composition CS/LN-09. Cs partitioned to an aluminotitanate phase in most of these samples. The alkaline earths, transition metals and some of the lanthanides also partitioned to titanate phases. The predicted $LnAlO_3$-type phases did not form using either fabrication method, which again may be due to a larger free energy of formation of these phases as compared to the titanates.

Partitioning of the Ce, Cs, La, and Pr in the Phase II CS/LN compositions was unclear from the XRD data. The Ce, La, and Pr may have partitioned to the perovskite phase as identified for some of the Phase I compositions. The EDS data showed these elements to be fairly well distributed throughout the material (see Figure 3-10).

Table 3-7. Summary of XRD Data for Phase II CS/LN Waste Forms Prepared by Two Methods.

Phases	Press and Sinter			Melt and Crystallize		
	CS/LN-06	CS/LN-08	CS/LN-09	CS/LN-06	CS/LN-08	CS/LN-09
$Sr_{0.34}Nd_{2.44}Ti_4O_{12}$				X	X	
$BaNd_2Ti_4O_{12}$			X	X		X
$BaAlTi_5O_{14}$ Hollandite	X	X		X	X	
$Nd_2Ti_2O_7$ Pyrochlore	X	X	X		X	X
$Cs_2Ti_2Al_2O_8$					X	X
$BaTiO_3$ perovskite	X	X	X			
Unreacted Al_2O_3		X	X			X (SEM/EDS)
$Ba_4(Sr_2Sm_8)(TiO_3)_{18}$		X	X			

XRD data for the Phase II CS/LN High Mo compositions prepared via two of the fabrication methods are summarized in Table 3-8. A broader range of phases were identified via XRD in these compositions. The Mo waste component was incorporated as $BaMoO_4$ in all of the compositions. Most of the samples contained an Nd pyrochlore phase and/or a hollandite-type phase. Various metal zirconate and metal titanate phases were detected in several of the compositions fabricated by both methods. Zirconolite phases were present in two of the compositions fabricated by pressing and sintering. Interestingly, a Ln-Al perovskite, originally predicted to form in these systems but not seen until this point, was detected in a small concentration in composition CS/LN/TM High Mo-09 fabricated by pressing and sintering. Composition CS/LN/TM High Mo-09 targeted a waste loading of 65%. This may indicate that there was not enough Ti available to completely form the more stable titanate phases. An additional difference observed in the Phase II compositions was the regular appearance of the targeted hollandite-type phases, which were not observed in any of the Phase I compositions. A small amount of CeO_2 was detected via XRD in this composition when fabricated by pressing and sintering, which may indicate that the waste loading limit has been exceeded at this level.

Composition CS/LN/TM High Mo-08 fabricated by pressing and sintering contained a phase that couldn't be identified using a search/match of the XRD data. The peaks representing this phase corresponded to d-spacings of approximately 2.51, 2.29, 1.82, 1.74 1.55, and 1.52 angstroms. All of the Phase II CS/LN/TM High Mo waste forms fabricated by melting and crystallizing included an unidentifiable phase as well. The peaks corresponding to this phase had fairly low relative intensities, and corresponded to d-spacings of approximately 3.48, 3.10, 2.51, 2.31, 1.74, and 1.52 angstroms. Further investigation using the SEM and EDS will be useful in identifying these phases.

No free Al_2O_3 was detected by XRD in the Phase II CS/LN/TM samples fabricated by either method, although it would be useful to use EDS to verify that no unreacted Al_2O_3 grains are present. Partitioning of the Ca, Ce, Cs, La, Nd, Pr, and Sm in the Phase II CS/LN/TM High Mo compositions was unclear from the XRD data. Additional characterization via SEM and EDS is needed to better understand partitioning of these elements. It may be unnecessary to add CaO to this waste stream since $BaMoO_4$ is forming more readily than powellite. Also, the compositions with the highest CaO content (CS/LN/TM High Mo-05 and -09) displayed the least amount of melting. Therefore, reducing the CaO concentration to be only enough to support formation of the Zr-containing phases may be beneficial for both processing as well as compositional optimization.

Table 3-8. Summary of XRD Data for Phase II CS/LN/TM High Mo Waste Forms Prepared by Two Methods.

Phases	Press and Sinter			Melt and Crystallize		
	CS/LN/TM High Mo-06	CS/LN/TM High Mo-08	CS/LN/TM High Mo-09	CS/LN/TM High Mo-06	CS/LN/TM High Mo-08	CS/LN/TM High Mo-09
$BaMoO_4$	X	X	X	X	X	X
$Nd_2Ti_2O_7$ pyrochlore		X	X	X	X	
$BaAlTi_5O_{14}$ hollandite	X			X	X	
$Al_{0.1}Zr_{0.9}O_{1.95}$				X	X	
$Nd_{0.25}Zr_{0.75}O_{1.875}$			X			X
$Ca_{0.61}La_{0.39}Al_{0.39}Ti_{0.61}O_3$						X
$La_{0.4}Ca_{0.4}TiO_3$ perovskite	X					
$Sm_2Ti_2O_7$ pyrochlore	X					
$CaZrTi_2O_7$ zirconolite	X					
$NdGdTi_2O_7$ zirconolite		X				
$Ce_{0.3}La_{0.7}AlO_3$			X			
CeO_2			X			

3.5.   Chemical Durability

The PCT was used to provide insight into the chemical durability of the waste forms fabricated by melting and crystallizing. The results can only be used as preliminary information since no benchmark materials exist for comparison.   Relationships between the rates of leaching of elements in non-radioactive waste forms of this type have not been related to the rates of leaching of actual radionuclides under the PCT conditions. For example, the Environmental Assessment (EA) glass was developed as a benchmark for the PCT with borosilicate waste glasses.[14] The leaching rate of boron in non-radioactive borosilicate glasses can be related to radionuclide release in actual high level waste glasses. No such benchmark composition is available for the aluminum and titanium-based ceramic waste forms in this study. However, the results can provide some measure of the ability of the ceramics to contain the simulated waste elements, and qualitative differences among the compositions studied can be identified.

Results of the PCT for the Phase I compositions fabricated by melting and crystallizing are given in Table 3-9. The numbers of replicates tested for each composition are also listed and were dependent on the amount of material available for the test. A review of Table 3-9 shows that the normalized leachate release rate for Al was much higher for the CS/LN compositions than for the CS/LN/TM High Mo compositions.   Releases of Ba and Ca were minimal.   The releases of Cs and Rb for all of the compositions are likely significant, but a benchmark is needed in order to better qualify the measurements. The Ti concentrations in the leachates were below the instrument detection limit. The standard sieve sizes were used in preparing the samples for the PCT, but a measurement of the true surface area of the material (due to potential differences in particle shape and porosity) would provide further insight into the test results.   Releases for Mo appear to be less significant, although still higher than the matrix components. In general, the CS/LN/TM High Mo compositions appear to be more durable than CS/LN compositions for the elements measured.   There are no clear trends in release rates for the elements measured among the three CS/LN compositions or among the four CS/LN/TM High Mo compositions.

Results of the PCT for the Phase II compositions fabricated by melting and crystallizing are given in Table 3-10. The measurements for Cs in the Phase II compositions had not been completed at the time of this report. These data will be reported in FY2011. Normalized release rates for Al were mixed, but were lower for the CS/LN/TM High Mo compositions. The normalized release rates for Ba and Ca in the CS/LN/TM High Mo compositions were very low.   The release rate for Mo was sharply lower for composition CS/LN/TM High Mo-09 compared to the other CS/LN/TM High Mo compositions, although this composition had the highest concentration of MoO_3 and all of the compositions formed the same $BaMoO_4$ phase. Release rates for Rb varied considerably among the Phase II compositions, with no clear compositional driver. The Ti concentrations in the leachates were below the instrument detection limit. Again, it is difficult to draw further conclusions from these data until a benchmark material is developed for the PCT with this type of waste form.   Further characterization should be performed to better understand the behavior of these materials in this durability test.

Table 3-9. Results of the PCT for the Phase I Compositions Fabricated by Melting and Crystallizing. Normalized Leachate Release Rates (g/L) are Given for Several Elements.

Composition	Number of Replicates	Al	Ba	Ca	Cs	Mo	Rb
CS/LN-03	2	3.10	b/d	-	44.09	-	8.73
CS/LN-04	2	3.48	b/d	-	32.36	-	4.78
CS/LN-05	2	3.04	b/d	-	44.83	-	8.67
CS/LN/TM Mo-02	1	0.03	0.08	0.05	38.04	5.61	20.48
CS/LN/TM Mo-03	1	0.03	0.18	0.04	28.12	9.62	13.23
CS/LN/TM Mo-04	1	0.03	0.27	0.03	23.73	7.68	10.49
CS/LN/TM Mo-05	1	0.03	0.03	0.01	25.13	6.06	10.18

Note: b/d indicates value was below the instrument detection limit

Table 3-10. Results of the PCT for the Phase II Compositions Fabricated by Melting and Crystallizing. Normalized Leachate Release Rates (g/L) are Given for Several Elements.

Composition	Number of Replicates	Al	Ba	Ca	Mo	Rb
CS/LN-06	1	0.17	b/d	-	-	b/d
CS/LN-08	1	2.06	b/d	-	-	7.08
CS/LN-09	1	1.37	b/d	-	-	5.36
CS/LN/TM High Mo-06	1	0.22	0.08	0.06	12.29	31.21
CS/LN/TM High Mo-08	1	0.15	0.03	0.03	13.32	46.52
CS/LN/TM High Mo-09	1	0.09	0.04	0.01	0.65	b/d

Note: b/d indicates value was below the instrument detection limit

3.6.   Radiation Damage Tolerance

A sample of composition CS/LN/TM High Mo-02 fabricated by melting and crystallizing was subjected to a 5 MeV He ion beam with a fluence of $1x10^{17}$ ions/cm^2 at room temperature to provide preliminary insight into the radiation damage tolerance of the ceramic waste forms. These conditions are estimated to produce damage up to a depth of about 10 µm within the material. The sample was evaluated by SEM and XRD before and after irradiation to identify any microstructural changes induced by the alpha bombardment. Figure 3-11 shows secondary and backscattered electron images of the specimen. As described earlier, this composition contains several crystalline phases, including unreacted Al_2O_3 (the dark, elongated grains in Figure 3-11b), as well as some porosity.

(a)   **(b)**
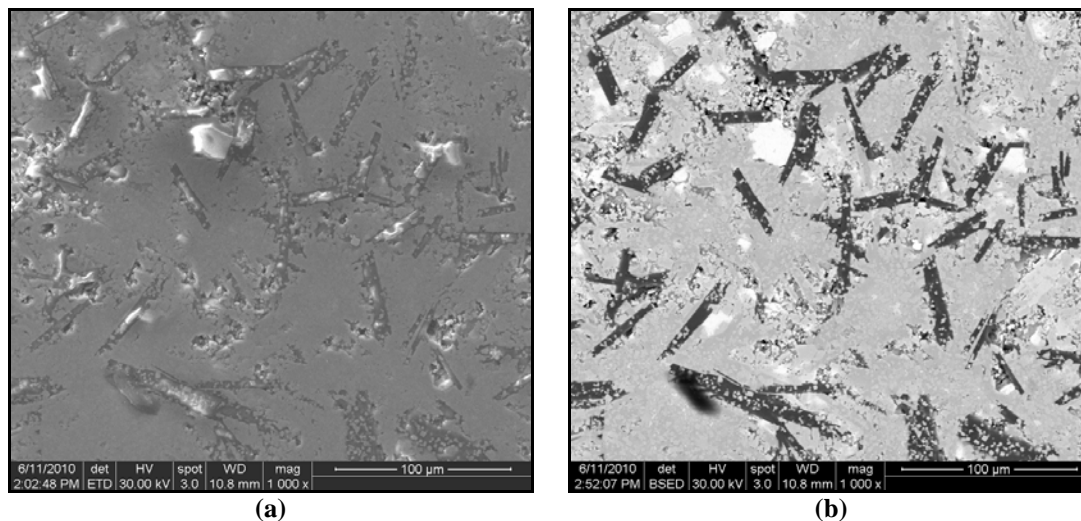
Figure 3-11. Secondary Electron (a) and Backscattered Electron (b) Micrographs of Composition CS/LN/TM High Mo-02 Prior to Ion Beam Irradiation.

Figure 3-12 shows similar micrographs of the specimen after ion beam irradiation. Comparison with the micrographs in Figure 3-11 shows no obvious changes in microstructure due to ion beam irradiation. The volume fraction and morphology of each phase appears unchanged, as well as the volume of void or pore space.

(a)   (b)
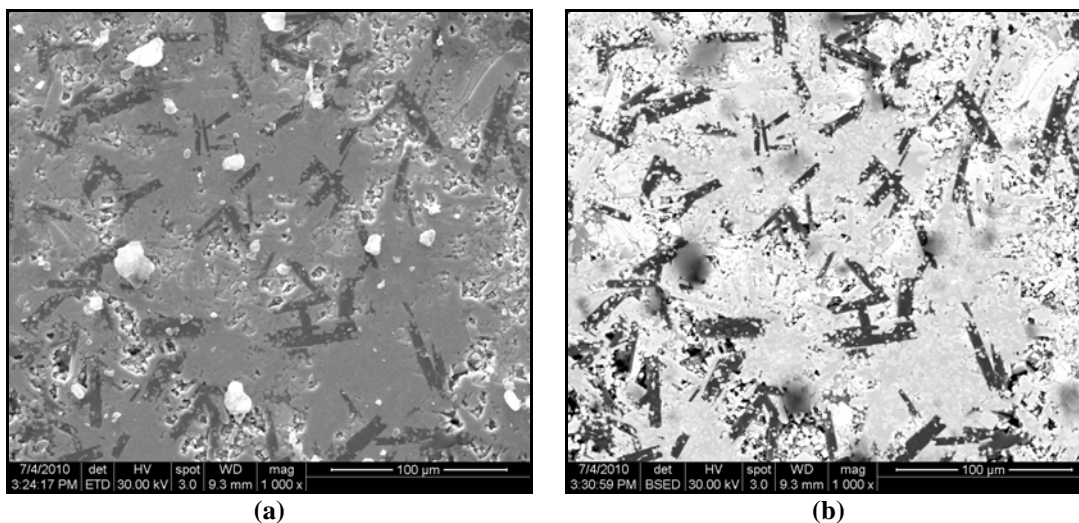
Figure 3-12. Secondary Electron (a) and Backscattered Electron (b) Micrographs of Composition CS/LN/TM High Mo-02 After Ion Beam Irradiation.

Figure 3-13 provides a comparison of XRD spectra of the surface of the sample of composition CS/LN/TM High Mo-02 obtained before and after the ion beam irradiation. There is very little difference between the two spectra, again providing a preliminary indication that this composition is resistant to radiation induced damage.
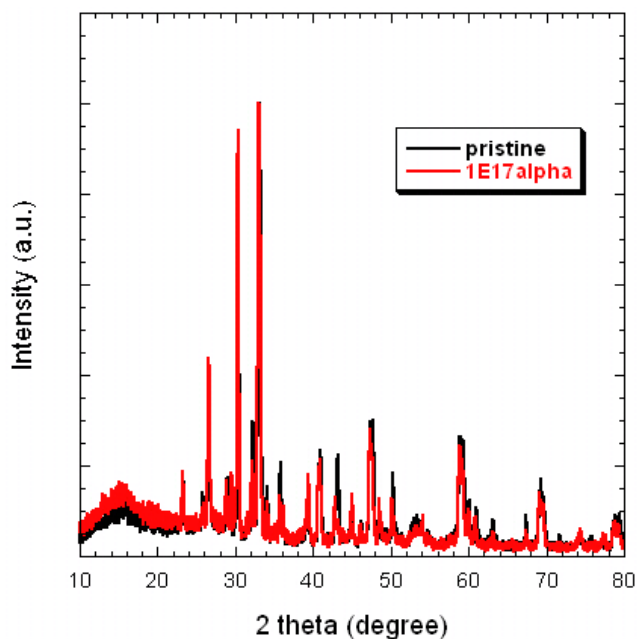
Figure 3-13. XRD Patterns for Composition CS/LN/TM High Mo-02 Prior to (pristine) and After (1E17alpha) Ion Beam Irradiation.

4. SUMMARY AND CONCLUSIONS

SRNL developed a series of ceramic waste forms for the immobilization of CS/LN and CS/LN/TM waste streams anticipated to result from nuclear fuel reprocessing. Simple raw materials, including Al_2O_3, CaO, and TiO_2 were combined with simulated waste components to produce multiphase ceramics containing hollandite-type phases, perovskites (particularly $BaTiO_3$), pyrochlores, zirconolite, and other minor metal titanate phases. Identification of excess Al_2O_3 via XRD and SEM/EDS in the first series of compositions led to a Phase II study, with significantly reduced Al_2O_3 concentrations and increased waste loadings.

Three fabrication methodologies were used, including melting and crystallizing, pressing and sintering, and SPS, with the intent of studying phase evolution under various sintering conditions. XRD and SEM/EDS results showed that the partitioning of the waste elements in the sintered materials was very similar, despite varying stoichiometry of the phases formed. The Phase II compositions generally contained a reduced amount of unreacted Al_2O_3 as identified by XRD. They also had phase assemblages that were closer to the initial targets, including hollandite phases in the CS/LN/TM High Mo compositions. Chemical composition measurements showed no significant issues with meeting the target compositions. However, volatilization of Cs and Mo was identified, particularly during melting, since sintering of the pressed pellets and SPS were preformed at lower temperatures. Partitioning of some of the waste components was difficult to determine via XRD. EDS mapping showed that these elements, which were generally those present in smaller concentrations, were well distributed throughout the waste forms.

Initial studies of radiation damage tolerance using ion beam irradiation showed little if any modification of the material after irradiation. Additional study in this area is needed. Chemical durability was briefly studied using the PCT. Most of the elements measured were retained very well by the ceramic waste forms, indicating good chemical durability. Cs, Mo, and Rb were released at somewhat higher rates as compared to the matrix, although benchmark compositions and further physical characterization, including density and surface area, are needed in order to qualify the PCT results.

5. FUTURE WORK

Characterization of the Phase II compositions will be completed early in FY2011, including Cs concentration measurements in support of the chemical composition and PCT data and SEM/EDS studies of select Phase II CS/LN/TM High Mo waste forms.

The majority of work in FY2011 will focus on two areas. The first objective will be the optimization of the melt and crystallization process with respect to phase assemblage with combined CS/LN/TM waste streams. The second objective will be to better understand phase formation and elemental partitioning within these multi-phase waste forms. Selected individual phases identified in this report will be synthesized individually by both melting and crystallizing, and pressing and sintering methodologies. Samples of the individual phases will be sent to LANL for SEM, EDS, EPMA, and TEM analyses, as well as ion irradiation studies. SRNL will lead this collaborative effort in order to improve the fundamental understanding of phase evolution and performance of the ceramic waste forms.

6. REFERENCES

1. Gombert, D., S. Piet, T. Trickel, J. Carter, J. D. Vienna and W. Ebert, "Combined Waste Form Cost Trade Study," *U.S. Department of Energy Report GNEP-SYSA-PMO-MI-DV-2009-000003,* Idaho National Laboratory, (2008).

2. Crum, J. V., A. L. Billings, J. Lang, J. C. Marra, C. Rodriguez, J. V. Ryan and J. D. Vienna, "Baseline Glass Development for Combined Fission Products Waste Streams," *U.S. Department of Energy Report AFCI-WAST-WAST-MI-DV-2009-000075,* Pacific Northwest National Laboratory, (2009).

3. Ringwood, A. E., E. S. Kesson, N. G. Ware, W. Hibberson and A. Major, "Geological Immobilisation of Nuclear Reactor Wastes," *Nature,* **278** 219 (1979).

4. Ringwood, A. E., E. S. Kesson, K. D. Reeve, D. M. Levins and E. J. Ramm, "Synroc," pp. 233-334 in *Radioactive Waste Forms for the Future,* W. Lutze and R. C. Ewing, eds. Elsevier, North-Holland, Amsterdam, Netherlands (1988).

5. Perera, D. S., B. D. Begg, E. R. Vance and M. W. A. Stewart, "Application of Crystal Chemistry in the Development of Radioactive Wasteforms," *Advances in Technology of Materials and Materials Processing,* **6** [2] 214-217 (2004).

6. Stefanovsky, S. V., A. G. Ptashkin, O. A. Knyazev, S. A. Dmitriev, S. V. Yudintsev and B. S. Nikonov, "Inductive Cold Crucible Melting of Actinide-bearing Murataite-based Ceramics," *Journal of Alloys and Compounds,* **444-445** 438-442 (2007).

7. Demine, A. V., N. V. Krylova, P. P. Polyektov, I. N. Shestoperov, T. V. Smelova, V. F. Gorn and G. M. Medvedev, "High Level Waste Solidification Using a Cold Crucible Induction Melter"; pp. 27-34 in Mater. Res. Soc. Symp. Proc., Vol. 663, *Scientific Basis for Nuclear Waste Management XXIV.* Edited by K. P. Hart and G. R. Lumpkin. Warrendale, PA, 2001.

8. Advocat, T., G. Leturcq, J. Lacombe, G. Berger, R. A. Day, K. Hart, E. Vernaz and A. Bonnetier, "Alteration of Cold Crucible Melter Titanate-based Ceramics: Comparison with Hot-Pressed Titanate-based Ceramic"; pp. 355-362 in Mater. Res. Soc. Symp. Proc., Vol. 465, *Scientific Basis for Nuclear Waste Management XX.* Edited by W. J. Gray and I. R. Triay. Pittsburgh, PA, 1997.

9. Leturcq, G., T. Advocat, K. Hart, G. Berger, J. Lacombe and A. Bonnetier, "Solubility Study of Ti Zr-based Ceramics Designed to Immobilize Long-lived Radionuclides," *American Mineralogist,* **86** [7-8] 871-880 (2001).

10. Collins, E., "Testing Results CETE, Waste Forms – TMFP Composition Video Conference," (November 19, 2008).

11. Bakel, A. J., D. L. Bowers, K. J. Quigley, M. C. Regalbuto, J. A. Stillman and G. F. Vandegrift, "Dissolution of Irradiated Nuclear Fuel from the Big Rock Point Reactor"; pp. 71-88 in ACS Symposium Series, Vol. 933, *Separations for The Nuclear Fuel Cycle in the 21st Century.* Edited by G. J. Lumetta, K. L. Nash, S. B. Clark and J. I. Friese. American Chemical Society, Washington, DC, 2006.

12. Saal, J. E., D. Shin, A. J. Stevenson, G. L. Messing and Z.-K. Liu, "First-Principles Calculations and Thermodynamic Modeling of the Al_2O_3-Nd_2O_3 System," *Journal of the American Ceramic Society,* **91** [10] 3355-3361 (2008).

13. Helean, K. B., S. V. Ushakov, C. E. Brown, A. Navrotsky, J. Lian, R. C. Ewing, J. M. Farmer and L. A. Boatner, "Formation Enthalpies of Rare Earth Titanate Pyrochlores," *Journal of Solid State Chemistry,* **177** [6] 1858-1866 (2004).

14. Jantzen, C. M., N. E. Bibler, D. C. Beam, C. L. Crawford and M. A. Pickett, "Characterization of the Defense Waste Processing Facility (DWPF) Environmental Assessment (EA) Glass Standard Reference Material," *U.S. Department of Energy Report WSRC-TR-92-346, Revision 1,* Westinghouse Savannah River Company, Aiken, SC (1993).